Global View of the Intraseasonal Oscillation during Northern Winter

Huang-Hsiung Hsu
Department of Atmospheric Sciences
National Taiwan University

Abstract

In this study, we applied SVD analysis to a normalized 200 mb streamfunction/OLR covariance matrix to extract the most recurrent coupled pattern in the northern winter, after the removal of the climatological seasonal cycle and seasonal means for each winter. The first two singular vectors are on an intraseasonal time scale and the combination of the two forms an oscillation. It is characterized by eastward propagation in the Indian Ocean and the western Pacific, standing oscillations in both the tropics and the extratropics, and the poleward propagation of a zonally symmetric structure.

Although there exists eastwardly propagating pattern, the phase relationship between geopotential, wind and streamfunction fields is inconsistent with that of equatorial Kelvin waves. Eastward propagation is most evident in the tropics of the Southern Hemisphere, while the signals in the Northern Hemisphere are characterized by standing oscillations. The distinct characteristics of the Northern and Southern Hemisphere can be attributed to the different properties of the mean flows which lead to distinct Rossby wave source distributions in the two hemispheres.

Abrupt developments of regional circulation anomalies are found in the exit regions of the Pacific and Atlantic jet streams. The one in the Pacific resembles the Pacific/North American pattern and develops in a process similar to the optimal excitation of the normal mode, by extracting barotropic energy from the mean flow. Similar energy conversion also occurs in the Atlantic. Both analyses of energy conversion and Rossby wave source indicate the occurrence of rigorous extratropical activity in the Northern Hemisphere, that may not be influenced directly by tropical heating. The propagating circulations in the Southern Hemisphere, that resemble equatorial Rossby waves, could be the direct response to the tropical heating, while the signals of standing oscillation are the mixed results of direct response to the tropical heating and internal dynamics in the extratropics.

The results show the complexity of the intraseasonal oscillation, involving equatorial wave dynamics, tropical-extratropical interactions, and eddy-mean flow interactions. The phenomenon is global and it is inadequate to treat the problem as either a purely tropical phenomenon or a purely extratropical phenomenon.

1. Introduction

Madden and Julian (1971,1972) applied spectral analysis to the sounding data of tropical stations in the Indian and the Pacific oceans, finding spectral peaks at a nearly 40-50 day period at many stations. The phase lags between the tropical stations indicated an east-west planetary scale circulation that propagates eastward along the equator. Hartmann and Gross (1988) and Hartmann and Michelsen (1989), applying spectral analysis to wind and rainfall data in the tropics and in India, found similar spectral peaks with a nearly 40-50 day period.

Multivariate analyses such as principal component analysis was subsequently applied to global

data sets to examine the spatial structure and time evolution of the intraseasonal oscillation. It was found, e.g., by Knutson and Weickmann (1987), that the eastward propagation of the intraseasonal oscillation can be described by the first two eigenvectors of the velocity potential that are in quadrature in both time and space. A similar structure was also found in the outgoing longwave radiation data, but this appeared mainly in the Indian Ocean and the western Pacific, e.g., Lau and Chan (1985). The composite life cycle of the intraseasonal oscillation shown in Knutson and Weickmann (1987) exhibits a streamfunction pattern accompanied by either active or inactive large scale convective activity, which has a zonal scale equivalent to wavenumber one and propagates eastward from the Indian Ocean into the western Pacific. A close examination of their results does not clearly support the idea of an eastwardly propagating pattern around the globe, except in the velocity potential field. The outgoing longwave radiation pattern decays rather quickly when it reaches the date line. The slow eastward moving streamfunction pattern also tends to stall in the eastern Pacific and is followed by the sudden development of a new pattern on a much larger zonal scale covering the southern Eurasian continent.

The discrepancy between the behavior of the velocity potential and other variables can be attributed to the over-smoothing effect of the inverse Laplacian operation on the divergence field. The centers of velocity potential do not necessarily correspond to the maximum divergence or convergence. Hsu et al. (1990) pointed out the inadequacy to interpret the evolution of the intraseasonal oscillation based on the velocity potential. They also suggested that the eastward movement of the pattern was not a smooth propagation with an almost constant speed; instead a sudden shift of the pattern may occur during the evolution. Weickmann and Khalsa (1990) examined the evolution of tropical convection and found similar behavior. Besides the eastwardly propagating signal, strong standing oscillations tend to occur in the western Pacific, central Africa and south America where active convection persists (e.g., in Hsu et al., 1990; Knutson and Weickmann, 1987). The standing signals, which may play an important role in the evolution of intraseasonal oscillation, have long been ignored in both empirical and theoretical studies over the past decades. A thorough examination of the relationship between the propagating and standing signals could yield important information for a better understanding of the intraseasonal oscillation.

Many theories have been proposed to explain the behavior of the tropical intraseasonal oscillation. Madden and Julian (1972) pointed out its similarity to the equatorial Kelvin wave because of the eastwardly propagating nature of the oscillation along the equator. The 40-50 day time scale is, however, much larger than the time scale of a dry Kelvin wave. Chang (1977) found that the inclusion of viscosity yielded a Kelvin mode with a time scale of 40-50 days. The Kelvin wave-CISK mechanism, taking into account the nonlinear heating effect, has been recently proposed by Lau and Peng (1987) and Chang and Lim (1988) among others. It states that the mechanism damps the Rossby wave and preferentially amplifies the Kelvin wave that slowly propagates eastward with the tropical heating. The mechanism, however, produces a time scale of 20-30 days, much shorter than the observed one. It also fails to offer a reasonable explanation for the passage of a Kelvin wave through the eastern Pacific where convective activity is weak. Sui and Lau (1989) included surface heat fluxes in their model to help sustain the wave in the eastern Pacific. However, the mechanism also shortens the time scale of the wave. Recently, Wang and Rui (1990) proposed frictional wave-CISK mechanism that is able to obtain an oscillation of reasonable time scale. The unstable mode is a Kelvin wave coupled with a damped Rossby wave, that grows due to the latent heating induced by the frictional moisture convergence in the boundary layer. Salby et al. (1994) and Hendon and Salby (1994) provided further simulated and empirical evidence to support the idea. The above theories are designed to explain the eastward propagation of the tropical oscillation, that is most evident in the velocity potential field but is not as clear in other fields, such as streamfunction, divergence, or OLR. What is more important, Kelvin-wave like structures, except in the velocity potential field, have not been well documented. Hsu et al. (1990) found little evidence of an equatorial

Kelvin wave in the 1985/86 intraseasonal oscillation events.

Emanuel (1987) and Neelin et al. (1987) proposed an evaporation-wind feedback mechanism to explain the eastward propagation. It states that in an easterly basic state the surface evaporation associated with the intraseasonal oscillation is preferentially enhanced to the east of the tropical convection because of the larger wind speed, and acts to destablize the atmosphere to the east of the tropical convection. The interaction between evaporation and circulation subsequently leads to the eastward propagation of the system. The mechanism strongly depends on the basic state. In the real atmosphere, surface westerlies prevail in the Indian Ocean and the western Pacific where intraseasonal oscillations exhibit strongest signals. Such a basic state does not favor an eastward propagation. However, the mechanism may work in the eastern Pacific where surface easterlies prevail.

The above theories focus on the characteristics of eastward propagation and are unable to explain the strong signals of standing oscillations. To do this Hu and Randall (1994) proposed a radiative-convective interaction. They found two moist-neutral states existing in a one-dimensional general circulation model: one with a strong temperature lapse rate and a lower moisture content and another one with a weaker lapse rate and more moisture. The radiative and convective processes drive one state towards the other and an oscillation with a period of around 50 days occurs. The theory suggests that an intraseasonal oscillation could occur simply because of the local effects even without taking planetary scale circulation into account.

Bladé and Hartmann (1993) used a two-level nonlinear model with a positive-only CISK-type cumulus heating parameterization in which CISK type instability occurs only when the sea surface temperature exceeds a critical value. A stable and an unstable region coexist in the model. In their study, local instability recurs on a time scale of 40 days, without the initiating effect of moist Kelvin waves as proposed in the Kelvin wave-CISK theory. The time scale depends on the growth and duration times of the convective episode together with the recharge time for the instability. They also found that the organization of an intraseasonal oscillation episode is related to quasi-stochastic forcing provided by the mid latitude baroclinic eddies.

Signals on an intraseasonal time scale are not restricted to the tropics. Strong intraseasonal signals in the extratropics have been reported by several studies, e.g., Lau and Phillips (1986), Ghil and Mo (1991a,b), Schubert and Park (1991), Hsu et al. (1990), among others. Lau and Phillips (1986) documented the time lag relationship between the extratropical wavetrains and tropical convection and suggested the coupling between the normal modes of the tropics and the extratropics. Ghil and Mo (1991) concluded that the extratropical stationary modes were not driven by the tropical convection and that the intraseasonal modes in the tropics and the extratropics are two independent oscillators. They, however, suggested that the two oscillators are coupled by extratropical wavetrains. Schubert and Park (1991) found that the tropical convection in the western Pacific has a strong influence on the extratropical mode in the Pacific, by modifying the zonal wind distribution. Their extratropical mode, which was also documented by Hsu and Lin (1992), resembles the PNA (Pacific/North America) pattern (Wallace and Gutzler, 1981) and was found to have an energy source in the extratropics. Therefore, the extratropical mode is not a wavetrain forced purely by tropical convection. In a case study, Hsu et al. (1990) also pointed out that the intraseasonal oscillation should not be seen as a purely tropical phenomenon and the tropical-extratropical interaction can play a key role in the time evolution of the oscillation.

The above theories based on tropical dynamics are not able to explain the existence of the extratropical mode and its coupling with the tropical convection. Jin and Ghil (1990) took a different approach and demonstrated that extratropical low-frequency osci-llations may arise from wave-wave interactions and topographic form drag. A similar extratropical oscillation was also present in an idealized general circulation model in which the tropical intraseasonal oscillation does not exist (Marcus et al., 1994). On the other hand, the observed circulation patterns were found to be closely related to tropical convection (e.g., in Knutson and Weickmann,1987). How well the nonlinear theory proposed by Ghil and his

collaborators can explain the observed features remains to be seen.

The observed extratropical intraseasonal mode also resembles the most unstable normal mode in a barotropic model, incorporating a zonally-varying climatological basic state. It was demonstrated by Simmons et al. (1983), using a barotropic model, that the prescribed divergence forcing in the India and Indochina region result in the largest response of a circulation structure resembling the most unstable normal mode. The results are consistent with the finding of the adjoint mode, which is a wave-like pattern over the India and Indochina and leads to the optimal excitation of the normal mode (e.g., Zhang,1988; Ferranti et al., 1990). The fact that the PNA-like structure grows through barotropic energy conversion from the mean flow is consistent with the finding of Schubert and Park (1991). Both theoretical and empirical results discussed above indicate the importance of the tropical-extratropical interaction in an intraseasonal oscillation. The tropical convection may not be responsible for the growth of the extratropical mode, but may have a triggering effect on the initiation of the mode.

In most of the previous empirical studies, the intraseasonal oscillations were often extracted from the velocity potential field, emphasizing the propagating feature. The importance of the standing oscillation and the extratropics has not been the focus of much discussion. The development of theories has accordingly emphasized the importance of the equatorial Kelvin wave, viewing the phenomenon as a purely tropical feature. In this paper, we shall investigate the phenomenon on a global perspective, demonstrating the importance of extratropical circulation compared to the equatorial waves. This study applies the singular value decomposition method to the combined streamfunction/OLR covariance matrix to extract the most important coupled mode for a reexamination of the life cycle of intraseasonal oscillation. Section 2 describes the data set and the analysis procedure. The time evolution of the OLR and the streamfunction patterns are reviewed in section 3. Section 4 discusses the existence of the Kelvin-wave-like structure in the intraseasonal oscillation and section 5 examines the relative import-ance of standing oscillations and zonally propagating features. Distribution and evolution of Rossby wave source are shown in section 6 to examine the divergent effect on rotational flow. An extratropical structure and its development associated with the standing oscillation are discussed in the section 7. There exist zonally-symmetric patterns in the intraseasonal oscillation that are presented in section 8. Finally, the conclusions are given in Section 9.

2. Data and analysis procedures

The data used in this study are the ECMWF (European Centre for Medium-Range Weather Forecast) initialized wind and geopotential height data at 200, 850, and 1000 hPa and outgoing longwave radiation (OLR) at 12Z for eight winters (defined as December, January, and February) from 1980/81 to 1987/88. The ECMWF data are on a 5° × 5° global grid and the OLR data are on a 5° × 5° grid between 40° N and 40° S. To emphasize the large scale structure, the OLR, divergence and vorticity fields were spatially smoothed using a T12 spectral filter proposed by Sardeshmukh and Hoskins (1984). A climatological-mean seasonal cycle and the seasonal mean for each winter were subtracted to remove a part of interannual variability and to reduce the influence of the changes in the ECMWF data assimilation system through the years. We then computed five-day running means to remove the high frequency variability.

Singular value decomposition (SVD) analysis as described in Bretherton et al. (1992) was then applied to the temporal covariance matrix between the normalized streamfunction at 200 hPa and the normalized OLR to retrieve the most recurrent coupled patterns. The direct outputs of SVD analysis include: (1) singular vectors describing spatial patterns, (2) expansion coefficients describing the temporal variation of singular vectors, (3) singular values representing the amount of variance explained by singular vectors. The singular vectors obtained in this way are essentially the homogeneous correlation maps named by Bretherton et al. (1992), that is the simultaneous correlation maps between the expansion coefficients and the corresponding fields. Instead of showing the singular

vectors, maps of lag correlation coefficient between the expansion coefficients of the first two OLR vectors and the various variables at various time lags were computed to examine the corresponding time evolution and spatial structures. The same analysis procedures were also applied to a 30-60 day band-pass filtered data set to examine the influence of higher and lower frequency variability on the results derived from 5-day mean data. The comparison indicates a consistency between the results derived from the two data sets. The results derived from the 5-day means will be shown here.

To test the significance of correlation coefficients between the expansion coefficients and the various fields, degrees of freedom (DOF) were estimated following the procedure used in Chen (1982). We examined the spatial distribution of the DOF for each correlation map and found the smallest number of the DOF to be around 60. For the sake of convenience, 60 degrees of freedom will be assumed for each grid point in every correlation map. To reject the null hypothesis of no correlation at the 0.02 and 0.05 significance levels using a two-tailed test, correlation coefficients have to be at least .3 and .25, respectively.

3. Time evolution of singular vector

The first and second singular vectors explain 36 and 12 per cent of the squared covariance of the combined normalized 200 hPa streamfunction/OLR covariance matrix, respectively. Time series of the expansion coefficients associated with the first two singular vectors are shown in Figure 1. They are characterized by strong intraseasonal variability. Higher frequency signals are also present in Figure 1, because only a climatological-mean seasonal cycle and the seasonal means for each northern winter were subtracted from the five-day running means. The first two singular vectors in this study are in quadrature in both time and space. An examination of the two time series presented in Figure 1 indicates that the second vector tends to lead the first vector by a quarter of a cycle.

Lag correlation maps from -15 day lag to 15 day lag are shown in Figure 2 to illustrate the time evolution of the first OLR and 200 hPa streamfunction vectors. The simultaneous correlation map (i.e., day 0, Figure 2d) is identical to the first OLR and 200 hPa streamfunction singular vectors obtained from SVD analysis, while the correlation map for 15 day lag (i.e., day 15, Figure 2g) corresponds to the second set of singular vectors but with reversed signs. If stringent filtering had been applied to isolate the 30-60 day oscillation, the patterns at day -15 should just be the mirror image of the patterns at day 15. In this study, the similarity between the patterns at day -15 and day 15 is marked. However, there are differences between the two because of the presence of signals whose period is not 30-60 day. Since the first two vectors have a phase lag of a quarter of cycle, we shall only show the lag correlation maps for the first vector. For the sake of convenience, the features shown in the correlation maps will be described by assuming that the expansion coefficients are positive. For example, negative (positive) correlation coefficients for the OLR indicate active (inactive) convection, and positive (negative) correlation coefficients for the streamfunction indicate clockwise (anti clockwise) circulation.

(1) OLR

The time evolution of the first OLR vector from day -15 to day 15 is shown in Figure 2 in a shading scheme, i.e., the hatched areas indicating where the correlation coefficients are greater than 0.2 and the stippled areas indicating where the correlation coefficients are less than -0.2. The absolute values of the maximum correlation in the large shaded regions are generally larger than 0.4. The largest correlation coefficient that occurs in the western Pacific at day 0 exceeds 0.8.

The sequence begins with an OLR pattern similar to the second OLR singular vector, with inactive convection in the maritime continent and active convection in the western Indian Ocean. The pair moves slowly eastward while the convection in the Indian Ocean strengthens reaching its largest amplitude (-0.82) at day 0 (Figure 2d). At the same time, the region of inactive convection moves to the western Pacific extending southeastward into the South Pacific Convergence Zone (SPCZ). The OLR anomaly in the Atlantic that was negative at day -15 now becomes

positive, indicating weakening convection.

From day 0 to day 15, the strong convection region continues to move from 115° E to 150° E. During the same period, the inactive convection region in the western Pacific decays abruptly between day 0 and day 5, while a new center appears between the dateline and 150° W. A new region of inactive convection also appears in the Indian Ocean and moves eastward. The time evolution indicates little evidence of eastward propagation beyond the date line. There is little evidence to indicate that the convective activity in Central and South America and the Atlantic is an eastward extension of the convective activity in the Pacific. Instead, it seems to develop in situ. The time evolution shown above resembles that shown in Knutson and Weickmann (1987).

(2) Streamfunction

The time evolution of the first 200 hPa streamfunction vector is shown in Figure 2. The anomalous circulation pattern at day -20 (not shown) resembles the pattern at day 5 (Figure 2e) but the signs are reversed. The circulation pattern over Asia and the northern Pacific disintegrates rapidly from day -20 to day -15 while the circulation pattern in the Western Hemisphere remains at its peak phase. At the same time, a weak wave-like structure emanating from Indochina appears in the northern Pacific while the convection to its southern end, i.e., in the South China sea and Indochina, is less active. The wave-like structure develops into a dipole straddling the exit region of the Pacific jet by day -5. The development is rather dramatic between day -10 and day -5. A dipole straddling the equator between 30° E and 150° E also develops during the same period. By day 0, a pattern similar to the first vector is fully developed. The structure resembles the global pattern shown in Hsu and Lin (1992) that was derived from one-point correlation statistics. The evolution of the pattern indicates a weakening of the jet stream in the Pacific, equatorial easterly anomalies from 40° W eastward to 135° E, and equatorial westerly anomalies from 150° E to 150° W. The global pattern develops in situ and there is little evidence to suggest an eastward propagation of the circulation from the Indian Ocean into the western Pacific. The abrupt development of the extratropical dipole in the north Pacific is a noteworthy feature that will be discussed further in the following sections. The same abrupt development can be seen in the composite of Knutson and Weickmann (1987) but was barely discussed.

At day 0, the dipole of the convection anomalies in the western Pacific and the Indian Ocean is well developed and is located equatorward of the cyclonic and anticyclonic couplets, i.e., the cyclonic couplet lay poleward of the inactive convection region and the anticyclonic couplet lay poleward of the active convection region. The phase relationship between the tropical convection activity and the subtropical circulation is, to some extend, consistent with the simulated atmospheric responses to tropical heating (Gill, 1980; Simmons, 1983; Ting and Sardeshmukh, 1993). On the other hand, the convection in the western Pacific has been inactive since day -20 while the anomalous circulation patterns in the northern extratropical Pacific do not develop until day -5. It raises a doubt whether the existence of extratropical circulation can be attributed solely to tropical forcing. This will be discussed further in the following sections.

A similar phase relationship does not hold in the Atlantic. For example, an inactive convection region is flanked by an anticyclonic couplet to the north and south at day 0. It is worth noting that these inactive convection regions can be traced back to day -10 when they were located off the equator and equatorward of the anticyclonic anomalies. The phase relationship indicates that the convection variations in the Atlantic region do not act as forcing to the off-the-equatorial circulation anomalies in the subtropics. Park and Schubert (1993) found that the convection may be forced by an extratropical wave-like structure emanating from the Pacific. However, a similar pattern was not evident in Figure 2. Reason for the discrepancy between two studies is not clear.

From day 0 to day 15, the circulation anomalies in the Eastern Hemisphere weaken while the active convection region moves into the western Pacific and starts to decay. The cyclonic couplet straddling the equator in the central Pacific and the accompanying inactive convection region in the equator drift slowly

eastward. Both the circulation and convection anomalies weaken before reaching Central America. During this period, a cyclonic circulation to the east of the Caribbean sea develops abruptly from day 0 to day 10. The circulation anomaly in the western Hemisphere exhibits a more zonal structure and a meridionally banded structure. However, the extratropical circulation anomalies are weaker than their counterparts in the low latitudes. A wave-like pattern similar to that at day -10, but with reversed signs appears in the northern Pacific by day 20 and develops into a pattern resembling the first singular vector by day 30 (not shown). As a whole, the evolution of the 200 hPa streamfunction pattern in the Northern Hemisphere is characterized by the in-situ developments of new centers, that appear successively downstream, while its counterpart in the Southern Hemisphere exhibits a stronger component of eastward propagation.

The time evolution of the 850hPa streamfunction pattern along with the OLR pattern is shown in Figure 3. At day -20, an anticyclonic couplet straddling the equator, restricted between 30° N and 30 ° S, appears in the Indian Ocean and the western Pacific (not shown). The pattern along with an inactive convection region moves eastward into the Pacific at day -15. By day -10, the pattern develops into an anticyclonic couplet with much larger zonal and meridional scales. The development of an anticyclonic circulation anomaly in the subtropical Pacific that is associated with the 200 hPa wave-like structure (Figure 2b) leads to the larger meridional scale. At the same time, a new cyclonic couplet appears poleward of the active convection in the western Indian Ocean. The 200 hPa tropical circulation pattern at the same period exhibits a structure that is in quadrature with the 850 hPa pattern. This suggests that the circulation pattern at this stage does not possess a deep, coherent vertical structure. By day 0, the anticyclonic couplet has crossed the entire Pacific, extending to South America, while a cyclonic couplet covers the Indian Ocean. The tight gradients along the equator suggest strong easterly anomalies in the Pacific and westerly anomalies in the Indian Ocean. The positive correlation maximum in the northern Pacific appears near (60° N, 180° E) and is in phase with the northern center of the extratropical dipole at 200 hPa (Figure 2d).

A comparison between the streamfunction patterns at 200 hPa and 850 hPa indicates an out-of-phase relationship in the low latitudes and an in-phase relationship in the extratropics. This suggests the presence of vertical structures similar to the first internal mode in the tropics and the external mode in the extratropics. The contrasting vertical phase relationship in the tropics and extratropics results in the larger meridional scale of the 850 hPa streamfucntion pattern in the Northern Hemisphere. At 850 hPa in the Northern Hemisphere, tropical circulations exhibit a meridional scale similar to that of equatorial waves. On the contrary, the 200hPa circulation exhibits a much larger meridional scale that is inconsistent with the characteristics of equatorial waves. Both 850hPa and 200hPa stream-function patterns in the tropics of the Southern Hemisphere exhibit strong signals and are out of phase, indicating a stronger vertical coupling than their counterparts in the tropics of the Northern Hemisphere. The different characteristics of tropical circulation in the Northern and Southern Hemisphere are interesting. It could result from different mechanisms that will be discussed in Section 6.

By day 5, the region of anticyclonic anomaly extends eastward into the Atlantic, as do the equatorial easterly anomalies. The couplet in the Indian Ocean moves eastward into the western Pacific from day 5 to day 20. The meridional scale of the dipole shrinks during the course. The pattern in the eastern Pacific becomes zonally elongated at day 10, exhibiting an in-phase relationship with the 200 hPa pattern in both the tropics and the extratropics. The vertical structure of tropical circulation has changed from an out-of-phase relationship in the western Pacific to an in-phase relationship in the eastern Pacific. It will be shown in Section 8 that the in-phase vertical structure becomes evident at day 5 when a zonally-symmetric circulation pattern starts to propagate northward from the equator. The existence of the zonally-symmetric pattern is evident in Figures 3f and g.

The time evolution of the 200 hPa and 850 hPa streamfunction patterns exhibit different characteristics. The 200 hPa pattern tends to develop in-situ, showing weak eastward propagation, while the time evolution of

the 850 hPa pattern clearly shows an eastward propagation, especially in the tropics of the Southern Hemisphere. The different characteristics of tropical circulation in the upper and lower troposphere and between the Northern and Southern Hemisphere imply that the circulation in the upper and lower troposphere does not always couple in a way similar to the first internal mode, as had been assumed in many previous studies.

4. Kelvin wave signature

Mechanism based on equatorial Kelvin wave has been proposed by many researchers as an explanation for the eastward movement of intraseasonal oscillation. It would be interesting to see whether a structure similar to the one in a Kelvin wave can be found in our calculation. One way to judge the existence of a Kelvin wave is to compare the spatial structure of the streamfunction with that of the geopotential height and zonal wind. For an idealized Kelvin wave, its geopotential height and zonal wind distributions are symmetric to the equator, e.g., the maximum and minimum are located at the equator, while its streamfunction distribution is anti-symmetric, i.e., the maximum and minimum are located off the equator. The geopotential height and zonal wind are in phase in a dry Kelvin wave, and exhibit a small phase shift in a moist Kelvin wave (Wang, 1988; Lau et al., 1988). If such a spatial structure is found in our results, there is a possibility that it could be the reflection of a Kelvin wave in the real atmosphere.

Lag-correlation maps for the eddy geopotential height at both 1000 and 850 hPa were computed. The results of both fields are very similar. Figures 4a-c show the time evolution of the 1000 hPa eddy geopotential height from day -10 to day 10 every 10th day. Zonal means were removed to reduce the masking effect of a zonally-symmetric pattern on the eddy structure. At day -10, positive height anomalies cover the Pacific, while negative height anomalies cover the Indian Ocean and the Eurasian continent. A comparison to the 850 hPa streamfunction shows the following features: the positive height anomaly is associated with an anticyclonic couplet off the equator and an easterly anomaly at the equator, while the negative height anomaly is associated with a cyclonic couplet off the equator and a westerly anomaly at the equator. The phase relationship between the height, wind, and streamfunction fields is inconsistent with the structure of equatorial Kelvin waves (e.g., Matsuno, 1967; Hendon, 1989).

By day 0, the off-the-equator positive correlation maximum in the southern Pacific has moved to the central Pacific while a narrow band of weak negative correlation appears on the equator and extends from the negative correlation region in the west all the way to Central America. A closer examination of the time evolution between day -10 and day 0 indicates that the weak negative correlation appears simultaneously across the Pacific basin and that there is no indication of eastward propagation originating in the western Pacific. From day 0 to day 10, the region of negative correlation in the southern Indian Ocean moves into the southern Pacific while the region of negative correlation in the equatorial Pacific strengthens and extends to the eastern Pacific. Overall, the correlation near the equator is weaker than off the equator. The off-the-equator maximums are located to the poleward side of the tropical convection fluctuations and tend to be in-phase with the streamfunction couplets. The phase relationship between the streamfunction and the height fields suggests the characteristics similar to Rossby waves.

It can be noted in Figure 4 that the region of negative correlation near the west coast of the American continent moves northward along the coast in the Northern Hemisphere and southward along the coast in the Southern Hemisphere. This behavior is similar to the characteristics of coastal Kelvin waves that propagate with the coastal topography to the right in the Northern Hemisphere and to the left in the Southern Hemisphere (Gill, 1977). The correlation, although statistically significant, is not high.

Similar correlation statistics were also computed for the eddy geopotential height at 200 hPa. The maps from day -10 to day 10 are shown in Figures 4d-f. Most of maximum and minimum correlation is evidently located off the equator and tends to be in phase with the 200 hPa streamfunction pattern shown in Figure 2. There is an indication of a local maximum

at the equator in the Eastern Hemisphere in Figures 4e,f, e.g., the negative correlation region over the equatorial Indian Ocean and the positive correlation region over the maritime continent. The wedge-like positive correlation region over the maritime continent is associated with the off-the-equator anticyclonic circulations, equatorial easterly anomalies, and active convection to the west at day 0. The phase relationship again is not consistent with the structure of an equatorial Kelvin wave. The off-the-equator positive correlation regions over South Asia and the southern Indian Ocean coincide with the anticyclonic couplet in Figure 2d.

Hovmöller diagrams of the lag-correlation coefficients for the eddy geopotential height and zonal wind fields, averaged between 5° N and 5° S, at 200 and 850 hPa are shown in Figure 5a and 5b, respectively, to summarize the phase relationship between the wind and height fields. At 200 hPa, the zonal wind and the height fields are out of phase in the central Pacific, in quadrature in the western Pacific, and in phase from 0 to 70° E. The phase relationship in the central and western Pacific is inconsistent with the characteristics of equatorial Kelvin waves. In the region from 0 to 70° E, the phase relationship is consistent with that of a Kelvin wave. The convective activity in the region, however, is weak. At 850 hPa, westerly (easterly) anomalies lag behind negative (positive) height anomalies by about a quarter of the cycle. The phase relationship again does not support the existence of equatorial Kelvin waves in the eastern Indian Ocean and western Pacific where the convection is most active.

5. Standing oscillation vs. zonal propagation

In this section, we examine the relative importance of zonally propagating features and standing oscillations. The Hovmöller diagrams shown in Figure 6 present the lag correlation coefficients between the expansion coefficient and the OLR, divergence and velocity potential fields, averaged between 5° N and 5° S, to show the time evolution of the respective field. The zonal means were subtracted to show zonal propagation more clearly. The lag correlation coefficients for OLR shown in Figure 6a indicate an eastward propagation of convective activity from 60° E to the dateline and a period of about 50 days. There is no evidence of eastward propagation beyond the dateline. A closer examination also indicates the tendency of tropical convection to amplify at certain longitudes. The recurrence of the positive and negative correlation centers at the same longitudes suggests the existence of standing oscillations, besides the eastward propagation. Standing oscillations are most noticeable near 45° E, 90° E-120° E, 150° E-180°, and 30° W-0°

The time evolution of the 200 hPa divergence shown in Figure 6b resembles the time evolution of the OLR, especially in the Indian Ocean, the western Pacific, and the Atlantic. Signals of standing oscillations are even more evident. While both the OLR and the 200 hPa divergence show eastward propagation from the Indian Ocean to the dateline, the time evolution of 850 hPa divergence in Figure 6c indicates that the eastward propagation occurs only between 110 ° E and 150° E. Standing oscillations in the Indian Ocean and in the western Pacific characterize the time evolution. On the whole, the OLR and 200 hPa exhibit a pattern whose evolution is different from the one at 850 hPa. The tropical circulation in the area seems to bear a vertical structure more complicated than the first internal mode in the tropical troposphere.

The time evolution of the velocity potential has been widely examined, to infer the eastward propagation of the tropical convection, and has been interpreted as an equatorial Kelvin wave. The Hovmöller diagram of the 200 hPa velocity potential shown in Figure 6d, like those shown in many previous studies, shows an eastward propagation of the signals around the globe. The impression one may have from the time evolution of the velocity potential is rather different from the time evolution of the OLR and the divergence fields shown above. The slope of the maximum correlation region in Figure 6d also yields a faster speed than that may be deduced based on Figures 6a-c. The misrepresentation of the velocity potential is obvious and its interpretation should be made with caution.

Standing oscillation signals are also evident in other fields. Shaded regions in Figure 7 indicate the

fluctuation of the eddy component of the zonal wind averaged between 5° N and 5° S. Its fluctuations tend to be in phase with the 200 hPa streamfunction averaged in the 10° N-20° N (Figure 7a) and 10° S-20° S (Figure 7b) latitudinal bands. The in-phase relationship suggests the dominance of rotational wind. Standing oscillations, especially evident in the Northern Hemisphere, seem to occur at all longitudes but are more evident near 20° E, 100° E, 180° E, 90° W, and 15° W. Propagating features are also noticeable. The eastward propagation that is most evident in the Southern Hemisphere occurs only in the longitudinal domain where the OLR and divergence patterns also propagate eastward. Around-the-globe propagation is again not evident in the Northern Hemisphere but is more evident in the Southern Hemisphere, although the signals are very weak in the Western Hemisphere. Besides the eastward propagation, a westward propagation between 120° W and 60° W in the Northern Hemisphere is evident both in the equatorial zonal wind and streamfunction (Figure 7a).

At 850 hPa, the zonal wind averaged between 5° N and 5° S (shaded areas in Figure 7c) and the streamfunction averaged between 10° N and 20° N (Figure 7c) also exhibit strong signals of standing oscillation that occurs mainly in the Indian Ocean and the western Pacific. However, the streamfunction averaged between 10° S and 20° S (Figure 7d) clearly exhibits an eastward propagation. The contrast between the time evolution of the streamfunction fields in the Northern and Southern Hemisphere is also evident in Figure 3.

6. Rossby wave source

As pointed out by Sardeshmukh and Hoskins (1988), the atmospheric response to the tropical divergence is determined by the distribution of Rossby wave source (hereafter, referred to as RWS) that depends on the relative position of the divergence and the absolute vorticity fields. In this section, we examine the evolution of the RWS to yield useful information to explain the contrasting time evolution between the circulation in the Northern and Southern Hemispheres, i.e., the relative importance of standing oscillation and propagation. Linearized vorticity equation can be written as follows.

$$\frac{\partial \zeta'}{\partial t} = -\overline{V_\psi}\cdot\nabla\zeta' - V_\psi'\cdot\nabla\bar{\zeta} - \nabla\cdot(V_\chi'\zeta) - \nabla\cdot(\overline{V_\chi}\zeta') \qquad (1)$$

where $\mathbf{V}_\psi$ and $\mathbf{V}\chi$ are rotational and divergent winds, respectively, and ζ represents the absolute vorticity. The prime and overbar denote the perturbation and climatological mean, respectively. Sum of the third and fourth terms is defined as RWS.

To computer the RWS, we first calculated the lag regression coefficients of the wind fields on the expansion coefficient, that was then multiplied by one standard deviation of the expansion coefficient. By doing that, we reconstructed the wind anomalies when the variation of the expansion coefficient is equal to one standard deviation. The anomalies can be seen as the composite weighted by the expansion coefficients shown in Figure 1. The approach adopted has been used in many studies, e.g., Wright et al. (1988), Kiladis and Weickmann (1992), Hendon and Salby (1994). Shown in Figure 8 are the reconstructed 200 hPa wind and streamfunction anomalies at day -5. Its close resemblance to the correlation pattern shown in Figure 2c is evident. Tropical circulations are slightly emphasized in the correlation maps, because of the normalization by smaller standard deviation. The reconstructed wind fields were used to compute RWS. An examination on RWS will provide information about the effect of the divergence flow when the circulation pattern shown above (e.g., Figure 8) prevails in the atmosphere.

The distribution of the RWS from day -15 to day 15 every 10th day is shown in Figure 9. A region of negative RWS over Japan appears to be stationary from day -15 to day 5. It is replaced by a region of positive RWS at day 15 while the region of negative RWS shifts to the date line. The evolution occurs concurrently with the evolution of the divergence field at 200 hPa. A north-south dipole over East Asia exists between day -15 and day 5 as shown in Figure 10. The divergence center over Japan, located near the Pacific subtropical jet core where relative vorticity is the largest, contributes to the RWS minimum. As the tropical convection in the western Pacific switches from its inactive phase to its active phase between day -10 and

day 10, the Rossby wave source over Japan also switches from negative sign to positive sign when the divergence is replaced by convergence.

Sardeshmukh and Hoskins (1988) noted the importance of the vorticity advection by divergent winds associated with prescribed tropical divergence, which was also confirmed by Hsu (1994). The RWS shown above, however, indicates weak forcing in the tropics and exhibits close correspondence with the local divergence and convergence in the extratropics. It follows that the forcing is largely contributed by the divergence effect and not by the advection of divergent winds. To demonstrate this, the two terms comprising RWS in Equation (1) were computed. The fourth term is negligible compared to the third term. The flux term associated with eddy divergent flow can be further decomposed into two terms, i.e., the divergence term and the advection term, as follows.

$$-\nabla\cdot(\mathbf{V}_\chi'\zeta') = -\bar{\zeta}\nabla\cdot\mathbf{V}_\chi' - \mathbf{V}_\chi'\cdot\nabla\bar{\zeta} \qquad (2)$$

Figures 11a,b shows the contribution of the first and second terms in the right hand side of the Equation (1) at day -5. The dominance of the divergence term over the advection term is evident. The contribution of the advection term by divergent winds occurs mainly in two regions where both the climatological relative vorticity and the divergence anomalies exhibit large gradient. It can be inferred from Figure 11 that the divergent wind anomalies in the region southwest of Japan are downgradient of mean absolute vorticity, resulting in positive RWS. At the same time, the divergent wind anomalies over northern India and Arabian Peninsula are upgradient of mean absolute vorticity, resulting in negative RWS. The contribution of the advection term is, however, much smaller than that of the divergence term. This result does not contradict the conclusion of Sardeshmukh and Hoskins (1988) because only tropical divergence was prescribed in their study. In the case of weak extratropical divergence, their conclusions can still be valid.

The vorticity advection by rotational flows, i.e., the first and second terms at the right hand side of Equation (1), at day -5 are shown in Figures 11c,d. The eddy vorticity advection by the mean flow tends to balance RWS in the middle latitudes. In the subtropics, especially near 30° N, the first and second terms tend to cancel out. By comparing Figures 11 a,c,d, one would notice that they are not in perfectly balanced condition, especially in the subtropical region where the amplitudes are large in Figure 11c. However, the residuals of the four terms at the right hand side of Equation (1) exhibit a spatial scale smaller than the scale of each term (not shown). The circulations seem to adjust quickly enough to nearly balance the effects of rotational and divergent flows, even in five-day running averages. We examined the vorticity budget for all pentads shown here and found similar balanced condition.

The divergence perturbation over Japan develops from a wave-like pattern emanating from the eastern Indian Ocean into the northern Pacific, which can be seen clearly in Figure 10a. The corresponding divergence pattern is in quadrature with the vorticity pattern in such a manner that the divergence (convergence) anomalies are located downstream of the positive (negative) vorticity anomalies. The existence of a north-south dipole of the divergence suggests a modulation of the local Hadley circulation by the intraseasonal oscillation. The divergence anomaly over the east coast of East Asia appears to be quasi-stationary and begins to weaken when the tropical divergence anomaly moves into the western Pacific at day 10. Its stationarity leads to a slow variation in the RWS distribution in the northern Pacific, shown in Figure 9. Because of the almost stationary divergence maximum in the extratropics, the distribution of the RWS in the northern Pacific is relatively insensitive to the position of tropical convection, and its variation is relatively small when compared to the variation of tropical convection in the western Pacific. The extratropical circulation therefore varies little, appearing to be stationary during the above period, and does not change significantly until the complete reversal of tropical convection and the local Hadley cell in the western Pacific.

While extratropical circulations are active in the Northern Hemisphere, circulations in the Southern Hemisphere, particularly in the lower troposphere, are mostly confined to the tropics. This contrast between

the Northern and Southern Hemisphere is also evident in the RWS distribution shown in Figure 9. In the Northern Hemisphere, the RWS in the extratropics overwhelms the RWS in the tropics because of the large vorticity and its gradient near the jet streams. In the Southern Hemisphere, the RWS in the extratropics no longer dominates the RWS in the tropics because of the jet stream that is much weaker. The RWS distribution at 850 hPa also shows similar contrasting behavior.

The above results are consistent with Jin and Hoskins (1995). They used a baroclinic model to examine the effect of basic flow on wave propagation and concluded that the atmospheric responses to the tropical heating are sensitive to the structure of the basic flow. For example, they found that equatorial waves, especially Kelvin waves, only play an important role in the simulations taking a resting atmosphere as the basic state. In a climatological zonally-symmetric basic state, the initial perturbation evolves into Rossby wavetrains that prevail mostly in the winter Hemisphere. A modal structure similar to the Pacific-North America pattern (PNA) appears in a realistic climatological-mean flow. Influences of the mean flow on the response to tropical heating were also demonstrated by Garcia and Salby (1987). By placing tropical forcing centered at 10°S in a January zonally symmetric mean flow, they showed that the responses in the Northern Hemisphere are predominantly extratropical and wave-like. On the contrary, the responses in the Southern Hemisphere are mostly restricted in the low latitudes and are elongated zonally, exhibiting a characteristic similar to equatorial Rossby waves. The equatorial Kelvin waves, although evident, are weak.

Our results seem to be consistent with the numerical studies described above. In this study, the extratropical signals associated with the intraseasonal oscillation are more prominent in the Northern Hemisphere where zonal asymmetry is strong, while the equatorial signals are more prominent in the Southern Hemisphere where the flow is predominantly zonal. The circulation patterns in the tropics of the Southern Hemisphere are likely to be the direct response to the tropical heating and move eastward coherently with the eastward propagation of tropical convective activity. The circulation patterns in the Northern Hemisphere are the mixture of direct response to the tropical heating and self adjustment between the divergent and rotational flows embedded in Rossby wave-like disturbances. The latter is possibly influenced by the internal dynamics in the extratropics, that will be discussed in the following sections.

7. Extratropical structure in the Northern Pacific

The weak wave-like structure emanating from the eastern Indian Ocean into the northern Pacific, shown in Figures 10a and b, appears to be linked to the convective region over the eastern Indian Ocean present during the same period. It develops into a PNA-like structure, which resembles the most unstable mode of the climatological 300 hPa mean flow (Simmons et al., 1983). It was shown in the paper that Rossby wave propagation from South Asia into the exit region of the Pacific jet, similar to the one seen in Figure 10a, led to the development of the modal structure. It was later found (e.g., Zhang, 1989; Ferranti et al., 1990) that the adjoint of the PNA-like normal mode is a wave-like structure over the Indochina and India. By placing either an initial vorticity perturbation or a divergence forcing resembling the adjoint mode in a barotropic model linearized about the 300 hPa January climatological flow (Zhang, 1989), a wave-like pattern resembling the one in Figures 10a and b developed and evolved into the PNA-like modal structure. Although the mode develops rapidly by extracting barotropic energy from the mean flow, the normal mode instability has been found too weak to be responsible for the growth. Instead, non-modal growth that also extracts energy from the mean flow, seems to be a more plausible mechanism (Zhang, 1989; Ferranti et al., 1990; among others).

The sudden development of the PNA-like structure from the weak wave-like structure exhibits similar characteristics of the model results and theory described above. To examine whether the above mechanism occurs in intraseasonal oscillations, we estimate the kinetic energy conversion from the mean flow to the transient eddies, based on the reconstructed wind anomalies described in the preceding section. The kinetic energy conversion is defined as follows.

$$C(\bar{K},K') = -\frac{\overline{u'^2}}{a\cos\phi}\frac{\partial\bar{u}}{\partial\lambda} - \frac{\overline{u'v'}}{a}\cos\phi\frac{\partial}{\partial\phi}\left(\frac{\bar{u}}{\cos\phi}\right)$$

$$-\frac{\overline{u'v'}}{a\cos\phi}\frac{\partial\bar{v}}{\partial\lambda} - \frac{\overline{v'^2}}{a}\frac{\partial\bar{v}}{\partial\phi} + \overline{v'^2}\bar{v}\frac{\tan\phi}{a} \qquad (3)$$

The results are shown in Figure 12, for day -10, day 0, and day 15. At day -15 (not shown), there is significant positive energy conversion over Indochina but not in the northern Pacific. By day -10 (Figure 12a), significant positive energy conversion is established both in Indochina and in the central northern Pacific. The distribution of energy conversion is in quadrature with the wave-like pattern in the vorticity field, e.g., in Figure 10b. The positive energy conversion in South Asia and the central northern Pacific reaches its peak value at day 0. Regions of maximum energy conversion are sandwiched between the east-west elongated circulation dipoles, e.g., in Figure 10d. The derived E vector defined by Hoskins et al. (not shown) point westward, upgradient of the climatological-mean zonal wind speed, indicating a barotropic energy conversion from the mean flow to eddies. Schubert and Park (1991) also concluded that the PNA-like pattern has its main energy source in the middle latidues. The consistency between our results and the above theory suggests that the weak wave-like structure observed in Figure 10a, which seems to be forced by the convective activity in the tropics, may trigger the modal structure that grows through barotropic instability.

Significant energy conversions do not appear in the Atlantic until day 5. By day 10, the energy conversion rate slows down in the Pacific but speeds up in the Atlantic. The energy conversion rate in the Atlantic peaks at day 15 (Figure 12c). The above results show that the largest energy conversions in the Pacific and over South Asia are followed by the largest energy conversion in the Atlantic about 15 day later. The sequence coincides with the abrupt development of local circulation anomalies in these two regions. A close examination of the 200 hPa vorticity pattern from day -5 to day 5 (Figures 10c,d,e) reveals the existence of a tropical wavetrain that emanates from the tropical Southern Hemisphere near the dateline, crosses the equatorial westerly wave duct (Webster and Holton, 1982; Hsu and Lin, 1992) northeastward into the Caribbean sea. The structure is also evident in the streamfunction and height fields. The positive correlation region to the north of Brazil later develops into an anomalous circulation in the subtropics of the northern Atlantic. It seems possible that the perturbation associated with the cross-equator wavetrain triggers barotropic instability, leading to the amplification of anomalous circulation in the region.

The PNA-like modal structure, found by Simmons et al. (1983), evolves into a modal structure similar to the Eastern Atlantic pattern (Wallace and Gutzler, 1981) through Rossby wave dispersion across North America. A similar evolution is not evident in the sequence shown in Figures 2 and 10. Although a weak wave-like structure can be seen across North America at day 0, the strongest signals of in-situ development in the Atlantic appear to the east of the Caribbean sea between the equator and 30° N (Figure 10f) and do not have a clear link with the wave-like pattern in the high latitudes.

8. Meridional propagation

In the results shown above, zonally symmetric structures are evident during the evolution of intraseasonal oscillation. To examine the evolution of the zonally symmetric structures more closely, we computed lag correlation coefficients between the expansion coefficients of the first OLR vector and the zonal means of various variables. Shown in Figures 13a,b are lag correlation coefficients for zonally averaged OLR, streamfunction and zonal wind at 200 hPa and 850 hPa. Northward propagation that occurs mainly between the equator and 30° N is evident in all three fields. Positive (negative) streamfunction anomalies are accompanied by easterly (westerly) anomalies and positive (negative) OLR anomalies to the south. Standing oscillations are also evident in all three fields. Signals at the equator and in the Southern Hemisphere primarily exhibit the characteristics of standing oscillation with little evidence of meridional propagation. A comparison between Figures 13 and 2 shows that the zonally elongated circulation anomalies in Figure 2 starts to develop when the zonally averaged streamfunction reached its peak at 30° N.

For the 850 hPa streamfunction and zonal wind fields shown in Figures 13c,d, northward

propagation is evident between the equator and 30° N but is much weaker than its counterpart at 200 hPa. It is worth noting that northward propagating components at 200 hPa and 850 hPa are in phase, indicating an equivalent barotropic vertical structure. A standing oscillation in the northern extratropics in Figure 13c appears to be the strongest signal at 850 hPa. The extratropical standing oscillations at 200 hPa and 850 hPa exhibit a phase lag in such a manner that the 200 hPa pattern leads the 850 hPa pattern by about 10 days.

The above results suggest the possibility of an interaction between zonally symmetric circulation and the eddies during the evolution of intraseasonal oscillations. The northward propagation of the zonally symmetric pattern starts when the perturbations of zonally-averaged OLR in the tropics are the largest, that is also when the convection in the Indian Ocean is either most active or most inactive. The characteristics of the zonally symmetric pattern discussed above are consistent with the findings of previous studies on atmospheric angular momentum. Anderson and Rosen (1983) found that quasi-periodic fluctuation in the atmospheric angular momentum, on the time scale of 40-50 days, is associated with a wave-like pattern in the zonally-averaged zonal wind. The pattern also exhibits an equivalent barotropic vertical structure with its largest amplitude near 200 hPa, and propagates poleward from the equator to 20° N and 20° S. The propagation is more evident in the Northern Hemisphere. A near standing pattern linked with the propagating feature is also found near 40° N in their study. Kang and Lau (1994) and Magaña (1993) reported similar findings. Magaña (1993) further found that the 40- and 50-day oscillations of the globally integrated angular momentum (GAM) are predominantly contributed by fluctuations in the tropics. The oscillations are highly correlated with tropical convective activity in such a manner that the GAM is maximum when convection strengthens in the western/central Pacific and weakens in the Indian Ocean. The results shown here are consistent with the findings of Magaña (1993). To understand the phenomenon, Anderson and Stevens (1987) analyzed normal modes of a zonally symmetric basic flow and found a northward propagating mode with a period of 30-90 days when the basic flow includes the Hadley circulation. It is possible that the evolution of tropical convective activity associated with intraseasonal oscillation initiates the poleward propagation, by modulating the fluctuation of the Hadley circulation. However, the mechanism that controls the phase-locking between the zonally symmetric component and eddy is not yet understood.

9. Concluding remarks

In this study, we re-examine the time evolution of intraseasonal oscillation during the northern winter. The results show the complexity of the phenomenon. It includes eastward propagation along the equator, standing oscillations in both the tropics and the extratropics, and the poleward propagation of a zonally symmetric structure. Significant signals were found in various variables in both the tropics and the extratropics. Evidence of vigorous tropical-extratropical interaction was also found. Most of the previous studies have treated the phenomenon as a purely tropical feature and may have missed some important aspects of the intraseasonal oscillation.

The eastward propagation of convective activity was observed from the Indian Ocean to the dateline. The corresponding circulation patterns are the anticyclonic and cyclonic circulation couplets located poleward of the active and suppressed tropical convection. Hsu et al. (1990), Jin and Hoskins (1995) have shown that these circulation couplets can be forced by tropical heating. They also noted that Gill-type response to tropical heating (Gill, 1980), derived from a rest basic state, can not be applied to explain the structure of the observed couplets and their relative position to the heating. Many theories, mostly based on Kelvin-wave CISK, have been proposed to explain the cause of the eastward propagation. In this study, however, we found little evidence of equatorial Kelvin wave, consistent with the findings of Nishi (1989) and Hsu et al. (1990). For example, the in-phase relationship between the height and wind fields in a Kelvin wave is not evident in the area where eastward propagation prevails. Furthermore, the amplitudes do not decay rapidly away from the tropics as the equatorial waves do. Instead, the perturbations are

predominantly associated with Rossby-wave type circulation in the subtropics.

The above conclusion seems to be at odds with a recent study by Hendon and Salby (1994) in which they interpreted the relationship between tropical circulation and convection according to frictional wave-CISK mechanism proposed by Wang and Rui (1990). Their results also compare favorably with the model results of Salby et al. (1994). Their study considered only eastward, wavenumber 1-3 signals and excluded the signals of standing oscillation whose importance can be seen by comparing their Figures 8c and 10. Although Kelvin wave signals were evident in their results, the actual amplitudes could be small. For example, the amplitude of the equatorial westerly or easterly, interpreted as the signature of the Kelvin wave, does not drop away from the equator as rapidly as it should be in an equatorial-trapped wave. The atmospheric responses in the modeling study of Salby et al. (1994) are mostly restricted in the tropics and exhibits weak amplitudes in the extratropics, in contrast to the large extratropical amplitudes of the intraseasonal oscillation documented by Hendon and Salby (1994). The broad meridional scales of the circulation shown both here and in Hendon and Salby (1994), together with the inconsistency between the observed and simulated features, suggest that the interpretation of the intraseasonal oscillation based solely on equatorial wave dynamics is inadequate and has left some important features unexplained. Instead, the distribution of RWS, which depends on the relative positions of the climatological-mean flow and divergence perturbation, is a better representation of forcing to induce proper atmospheric responses.

Besides the eastward propagation, there is a tendency for circulation patterns and tropical convective activities to be amplified in certain regions, indicating the existence of standing oscillations. Signals of large amplitudes are present in both the tropics and the extratropics. While eastward propagation dominates the evolution of tropical convection and circulation patterns in the low latitudes of the Southern Hemisphere, standing oscillations are the dominant features for circulation patterns in the Northern Hemisphere. Extratropical signals are also much stronger in the Northern Hemisphere than in the Southern Hemisphere. This contrasting behavior seems to result from the different properties of the mean flow in the winter and summer hemisphere. It has been shown in several studies, e.g., Sardeshmukh and Hoskins (1989) and Hsu (1994), that remote responses in the subtropics and extratropics of the winter Hemisphere are relatively insensitive to the position of a specified tropical divergence. The RWS that induces the atmospheric circulation tends to reach its peak value near the core of the jet streams, as long as there exists absolute vorticity advection by divergent winds, or a local divergence anomaly near the relative vorticity maximum. In the winter Hemisphere, the relative vorticity and its gradient are very large near the jet streams and thus the Rossby wave source in the extratropics overwhelms the forcing in the tropics. This effect is less significant in the summer Hemisphere where the tropical forcing is not necessarily smaller than its extratropical counterpart, especially in the lower troposphere. It is thus understandable that the largest circulation signals in the Southern Hemisphere are in the tropical region and move eastward along with the tropical convection activity. Jin and Hoskins (1995) also showed that extratropical responses to tropical heating are more rigorous in the Northern Hemisphere than in the Southern Hemisphere during boreal winter.

It is found in this study that the RWS distribution in an intraseasonal oscillation is dominated by the local divergence effect, instead of by the advection of divergent flows as suggested in Sardeshmukh and Hoskins (1989). The extratropical circulation patterns in the Northern Hemisphere shown here exhibit Rossby wave-like characteristics. The divergence and vorticity fluctuations are in quadrature spatially in such a manner that divergence (convergence) anomalies lead positive (negative) vorticity anomalies. The divergence pattern embedded in the wave-like structure, together with the large relative vorticity near the jet stream, contributes significant RWS and overwhelms the contribution of advection effect. Before the abrupt development of the dipole in the northern Pacific, a wave-like pattern, which could be a stationary response to the tropical convective activity, emanates from Indochina into the northern Pacific. Its divergence

predominantly associated with Rossby-wave type circulation in the subtropics.

The above conclusion seems to be at odds with a recent study by Hendon and Salby (1994) in which they interpreted the relationship between tropical circulation and convection according to frictional wave-CISK mechanism proposed by Wang and Rui (1990). Their results also compare favorably with the model results of Salby et al. (1994). Their study considered only eastward, wavenumber 1-3 signals and excluded the signals of standing oscillation whose importance can be seen by comparing their Figures 8c and 10. Although Kelvin wave signals were evident in their results, the actual amplitudes could be small. For example, the amplitude of the equatorial westerly or easterly, interpreted as the signature of the Kelvin wave, does not drop away from the equator as rapidly as it should be in an equatorial-trapped wave. The atmospheric responses in the modeling study of Salby et al. (1994) are mostly restricted in the tropics and exhibits weak amplitudes in the extratropics, in contrast to the large extratropical amplitudes of the intraseasonal oscillation documented by Hendon and Salby (1994). The broad meridional scales of the circulation shown both here and in Hendon and Salby (1994), together with the inconsistency between the observed and simulated features, suggest that the interpretation of the intraseasonal oscillation based solely on equatorial wave dynamics is inadequate and has left some important features unexplained. Instead, the distribution of RWS, which depends on the relative positions of the climatological-mean flow and divergence perturbation, is a better representation of forcing to induce proper atmospheric responses.

Besides the eastward propagation, there is a tendency for circulation patterns and tropical convective activities to be amplified in certain regions, indicating the existence of standing oscillations. Signals of large amplitudes are present in both the tropics and the extratropics. While eastward propagation dominates the evolution of tropical convection and circulation patterns in the low latitudes of the Southern Hemisphere, standing oscillations are the dominant features for circulation patterns in the Northern Hemisphere. Extratropical signals are also much stronger in the Northern Hemisphere than in the Southern Hemisphere. This contrasting behavior seems to result from the different properties of the mean flow in the winter and summer hemisphere. It has been shown in several studies, e.g., Sardeshmukh and Hoskins (1989) and Hsu (1994), that remote responses in the subtropics and extratropics of the winter Hemisphere are relatively insensitive to the position of a specified tropical divergence. The RWS that induces the atmospheric circulation tends to reach its peak value near the core of the jet streams, as long as there exists absolute vorticity advection by divergent winds, or a local divergence anomaly near the relative vorticity maximum. In the winter Hemisphere, the relative vorticity and its gradient are very large near the jet streams and thus the Rossby wave source in the extratropics overwhelms the forcing in the tropics. This effect is less significant in the summer Hemisphere where the tropical forcing is not necessarily smaller than its extratropical counterpart, especially in the lower troposphere. It is thus understandable that the largest circulation signals in the Southern Hemisphere are in the tropical region and move eastward along with the tropical convection activity. Jin and Hoskins (1995) also showed that extratropical responses to tropical heating are more rigorous in the Northern Hemisphere than in the Southern Hemisphere during boreal winter.

It is found in this study that the RWS distribution in an intraseasonal oscillation is dominated by the local divergence effect, instead of by the advection of divergent flows as suggested in Sardeshmukh and Hoskins (1989). The extratropical circulation patterns in the Northern Hemisphere shown here exhibit Rossby wave-like characteristics. The divergence and vorticity fluctuations are in quadrature spatially in such a manner that divergence (convergence) anomalies lead positive (negative) vorticity anomalies. The divergence pattern embedded in the wave-like structure, together with the large relative vorticity near the jet stream, contributes significant RWS and overwhelms the contribution of advection effect. Before the abrupt development of the dipole in the northern Pacific, a wave-like pattern, which could be a stationary response to the tropical convective activity, emanates from Indochina into the northern Pacific. Its divergence

center over Japan is located near the jet core and leads to stationary Rossby wave source. The accompanying vorticity perturbation is a north-south dipole straddling the exit of the Pacific jet stream that is oriented in such manner to roughly balance the RWS through vorticity advection by mean rotational flows. The polarity of the dipole does not change until tropical convection in the western Pacific and the local Hadley circulation switches between its active and suppressed phases. It is suggested that the standing oscillations documented above are partly the manifestation of the extratropical quasi-stationary waves.

The circulation dipole in the northern Pacific and the variation of local Hadley circulation in East Asia develop from a wave-like structure emanating from the eastern Indian Ocean into the northern Pacific. A calculation of barotropic energy conversion suggests that the abrupt development of the anomalous circulation can be attributed, at least partially, to the local barotropic energy conversion from the time-mean flow to eddy. Although the PNA-like pattern is similar to the structure of the most unstable mode as suggested in Simmons et al. (1983), it has been shown recently that the normal-mode instability is too weak when compared to the non-modal growth or optimal excitation (Zhang, 1989; Ferranti et al., 1990; among others). It is worth noting that the development of the observed dipole resembles the process simulated in the barotropic model (Zhang, 1989).

The abrupt development of the circulation pattern in the exit region of the Atlantic jet stream is also associated with a similar energy conversion process. The circulation pattern in the northern Atlantic starts developing 10 days after the circulation pattern in the northern Pacific reaching its mature stage. In between, a wave-like structure in the upper troposphere emanates from the tropics of the southern central Pacific, crosses the westerly wave duct in the tropics of the eastern Pacific, and propagates into the Caribbean sea. It is likely that the perturbation associated with the wave pattern initiates the energy conversion, leading to the amplification of the circulation pattern. The proposed triggering effect has not been reported in any numerical or theoretical studies.

The above discussion suggests the possible role of tropical heating to force a stationary Rossby wave which in turn triggers a PNA-like structure through barotropic energy conversion from mean flows. However, we did not find concrete evidence of a two-way tropical-extratropical interaction. For example, the extratropical effects on tropical convection, suggested by Hsu et al. (1990) and Kiladis and Weickmann (1992), were not evident in this study. It is possible that the extratropical effects on tropical convection are most evident in the eastern Pacific where Rossby waves are allowed to penetrate into the tropics (Hsu and Lin, 1992; Tomas and Webster, 1994) but intraseasonal signals are weak. Kiladis et al. (1992) also found that such extratropical effects occur mostly in the disturbances of bi-weekly time scale, not in the intraseasonal time scale defined here. Whether scale interaction is important in an intraseasonal oscillation is not yet clear.

One of the difficult question for this study to answer is the relative importance of the tropical forcing and extratropical dynamics. As discussed above, a Rossby wave can be excited by tropical forcing. However, its internal dynamics can dominate the later evolution away from the tropics. It will be difficult to delineate their relative contributions. But, what we can be sure is that tropical forcing alone can not have excited the circulation features documented in this study. This argument is also implied in many studies of non-modal dynamics discussed above.

Another major question this study can not answer is the link between the eastward propagation of the tropical convection and the extratropical dynamics. This study confirms the eastward propagation of the tropical convection from the Indian Ocean to the western Pacific and points out the importance of the internal dynamics in the extratropics. On the other hand, we also find little evidence of equatorial Kelvin waves. Hendon and Salby (1994) have gone a step further to isolate eastward propagating component. Given the strict procedure they have applied, discrepancies between the filtered circulation pattern and the structure of equatorial waves remain. It seems likely that the signatures they extracted contained much more information than just equatorial waves. If a signal has to be obtained through complicated procedure, its amplitude could be very small. The study of Jin and

Hoskins (1995) implies the same argument. Based on this study, we can not suggest any new mechanism to explain the eastward propagation of the tropical convection. The leap-frog effect of the extratropical Rossby waves on the tropical convection, proposed by Hsu et al. (1990), was not evident in this study. It is possible that equatorial waves like Kelvin wave, although weak, can still have a triggering effect.

The northward propagation of zonally symmetric patterns occurs when the tropical convection in the Indian Ocean reaches its peak in the active and suppressed phases, and the zonally-averaged OLR anomalies have their extreme values. This feature is likely to be the normal mode of an intraseasonal time scale in a zonally symmetric mean flow that includes the Hadley circulation, as proposed by Stevens and Anderson (1987). The zonally symmetric pattern, which is also associated with the fluctuations of atmospheric angular momentum, is phase locked with the eddy components and tropical convection activity. The role of wave-mean flow interaction is an important aspect of the intraseasonal oscillation that has not yet been carefully examined and deserves further study.

The above discussion suggests that the intraseasonal oscillation is a global phenomenon and can not be treated either as a purely tropical or a purely extratropical feature. The phenomenon is much more complicated than what has been suggested by previous empirical and theoretical studies. The equatorial wave mechanism may explain some characteristics of the phenomenon, e.g., the eastward movement of the tropical convection activity. However, it fails to explain significant circulation features in the subtropics and extratropics. Evidently, theories based mainly on equatorial wave dynamics can only partially explain the evolution of the intraseasonal oscillation. Mechanisms considering tropical-extratropical interactions, extratropical internal dynamics and equatorial wave dynamics should be integrated to better understand the phenomenon.

Acknowledgment

This work was supported by the National Science Council of Taiwan under grant NSC82-0202-M002-074

References

Anderson, J. R., and R. D. Rosen, 1983: The latitude-height structure of 40-50 day variations in atmospheric angular momentum. *J. Atmos. Sci.*, **40**, 1584-1591.

Anderson, J. R., and D. Stevens, 1987: The presence of linear wavelike modes in a zonally symmetric model of the tropical atmosphere. *J. Atmos. Sci.*, **44**, 2115-2127.

Bladé, I., and D. L. Hartmann, 1993: Tropical intraseasonal oscillations in a simple nonlinear model. *J. Atmos. Sci.*, **50**, 2922-2939.

Bretherton, C. S., C. S. Smith, and J. M. Wallace, 1992: An intercomparison of methods for finding coupled patterns in climate data. *J. Climate*, **5**, 541-560.

Chang, C.-P., and H. Lim, 1988: Kelvin wave-CISK: a possible mechanism for the 30-50 day oscillations. *J. Atmos. Sci.*, **45**, 1709-1719.

Chen, W. Y., 1982: Fluctuations in Northern Hemisphere 700 mb height field associated with the Southern Oscillation. *Mon. Wea. Rev.*, **110**, 808-823.

Emanuel, E. A., 1987: An air-sea interaction model of intraseasonal oscillations in the tropics. *J. Atmos. Sci.*, **44**, 2324-2340.

Ferranti, L., T. N. Palmer, F. Molteni, and E. Klinker, 1990: Tropical-extratropical interaction associated with the 30-60 day oscillation and its impact on medium and extended range prediction. *J. Atmos. Sci.*, **47**, 2177-2199.

Garcia, R. R., and M. L. Salby, 1987: Transient response to localized episodic heating in the tropics. Part II: far field behavior. *J. Atmos. Sci.*, **44**, 499-530.

Ghil, M., and K. Mo, 1991: Intraseasonal oscillations in the global atmosphere. Part I: Northern Hemisphere and tropics. *J. Atmos. Sci.*, **48**, 752-779.

Ghil, M., and K. Mo, 1991: Intraseasonal oscillations in the global atmosphere. Part II: Southern Hemisphere. *J. Atmos. Sci.*, **48**, 780-790.

Gill, A. E., 1977: Coastally trapped waves in the atmosphere. *Quart. J. Roy. Meteor. Soc.*, **103**, 431-440.

Gill, A. E., 1980: Some simple solutions for heat-induced tropical circulation. *Quart. J. Roy. Meteor. Soc.*, **106**, 447-462.

Gutzler, D. S., and R. A. Madden, 1993: Seasonal variations of the 40-50 day oscillation in atmospheric angular momentum. *J. Atmos. Sci.*, **50**, 850-860.

Hartmann, D. L., and M. L. Michelsen, 1989: Intraseasonal periodicities in Indian rainfall. *J. Atmos. Sci.*, **46**, 2838-2862.

Hartmann, D. L., and J. R. Gross, 1988: Seasonal variability of the 40-50 day oscillation in wind and rainfall in the tropics. *J. Atmos. Sci.*, **45**, 2680-2702.

Hendon, H. H., and M. L. Salby, 1994: The life cycle of the Madden-Julian Oscillation. *J. Atmos. Sci.*, **51**, 2225-2237.

Hoskins, B. J. and F.-F. Jin, 1991: The initial value problem for tropical perturbations to a baroclinic atmosphere. *Quart. J. Roy. Meteor. Soc.*, **117**, 299-317.

Hsu, H.-H., B. J. Hoskins, and F.-F. Jin, 1990: The 1985/86 intraseasonal oscillation and the role of the extratropics. *J. Atmos. Sci.*, **47**, 832-839.

Hsu, H.-H. and S.-H. Lin, 1992: Global teleconnections in the 250-*hPa* streamfunction field during the Northern Hemisphere winter. *Mon. Wea. Rev.*, **120**, 1169-1190.

Hsu, H.-H., 1994: Relationship between tropical heating and global circulation: Interannual variability. *J. Geophys. Res.*, **99**, 10,473-10489.

Hu, Q., and D. R. Randall, 1994: Low-frequency oscillations in radiative-convective systems. *J. Atmos. Sci.*, **51**, 1089-1099.

Jin, F., and M. Ghil, 1990: Intraseasonal oscillations in the extratropics: Hopf bifurcation and topographic instabilities. *J. Atmos. Sci.*, **47**, 3007-3022.

Jin, F., and B. J. Hoskins, 1995: The direct response to tropical heating in a baroclinic atmosphere. *J. Atmos. Sci.*, **52**, 307-319.

Kang, I.-S., and K.-M. Lau, 1994: Principal modes of atmospheric circulation anomalies associated with global angular momentum fluctuations. *J. Atmos. Sci.*, **51**, 1194-1205.

Kiladis, G. N., and K. M. Weickmann, 1992: Extratropical forcing of tropical Pacific convection during northern winter. *Mon. Wea. Rev.*, **120**, 1924-1938.

Knutson, T. R., and K. M. Weickmann, 1987: The 30-60 day atmospheric oscillations: Composite life cycles of convection and circulation anomalies. *Mon. Wea. Rev.*, **115**, 1407-1436.

Lau, K.-M., and P. H. Chan, 1985: Aspects of the 40-50 day oscillation during the Northern winter as inferred from outgoing longwave radiation. *Mon. Wea. Rev.*, **113**, 1889-1909.

Lau, K.-M., and T. J. Phillips, 1986: Coherent fluctuations of extratropical geopotential height and tropical convection in intraseasonal time scales. *J. Atmos. Sci.*, **43**, 1164-1181.

Lau, K.-M., and L. Peng, 1987: Origin of low-frequency (intraseasonal) oscillations in the tropical atmosphere. Part I.: Basic theory. *J. Atmos. Sci.*, **44**, 950-972.

Lau, N.-C., I. M. Held and J. D. Neelin, 1988: The Madden-Julian oscillation in an idealized general circulation model. *J. Atmos. Sci.*, **45**, 3810-3832.

Madden, R. A., and P. R. Julian, 1972: Description of global-scale circulation cells in the tropics with a 40-50 day period. *J. Atmos. Sci.*, **29**, 1109-1123.

Magaña, V., 1993: The 40- and 50-day oscillations in atmospheric angular momentum at various latitudes. *J. Geophys. Res.*, **98**, **D6**, 10441-10450.

Marcus, S. L., M. Ghil, J. O. Dickey, 1994: The extra-tropical 40-day oscillation in the UCLA general circulation model. Part I: Atmospheric angular momentum. *J. Atmos. Sci.*, **51**, 1431-1446.

Neelin, J. D., I. M. Held, and K. H. Cook, 1987: Evaporation-wind feedback and low-frequency variability in the tropical atmosphere. *J. Atmos. Sci.*, **44**, 2341-2348.

Nishi, N., 1989: Observational study on the 30-60 day variations in the geopotential and temperature fields in the equatorial region. *J. Meteor. Soc. Japan*, **67**, 187-203.

Park, C.-K., and S. D. Schubert, 1993: Remotely forced intraseasonal oscillations over the tropical Atlantic. *J. Atmos. Sci.*, **50**, 89-103.

Rosen, D. R., D. A. Salstein, and T. M. Wood, 1991: Zonal contributions to global momentum variations on intraseasonal through interannual time scales. *J. Geophys. Res.*, **93**, **D3**, 5145-5151.

Salby M., R. Garcia, and H. Hendon, 1994: Planetary circulations in the presence of climatological and wave-induced heating. *J. Atmos. Sci.*, **51**, 2344-2367.

Sardeshmukh, P. D., and B. J. Hoskins, 1984: Spatial smoothing on the sphere. *Mon. Wea. Rev.*, **112**, 2524-2529.

Sardeshmukh, P. D., and B. J. Hoskins, 1988: The generation of global rotational flow by steady idealized tropical divergence. *J. Atmos. Sci.*, **45**, 1228-1251.

Schubert, S. D., and C.-K. Park, 1991: Low-frequency intraseasonal tropical-extratropical interactions. *J. Atmos. Sci.*, **48**,629-650.

Strong, C. M., F.-F. Jin and M. Ghil, 1993: Intraseasonal variability in a barotropic model with seasonal forcing. *J. Atmos. Sci.*, **50**, 2965-2986.

Sui, C.-H., and K.-M. Lau, 1989: Origin of low-frequency (intraseasonal) oscillations in the tropical atmosphere. Part II: Structure and propagation of mobile wave-CISK modes and their modification by lower boundary forcings. *J. Atmos. Sci.*, **46**, 37-56.

Tomas, R. A., and P. J. Webster, 1994: Horizontal and vertical structure of cross-equatorial wave propagation. *J. Atmos. Sci.*, **51**, 1417-1430.

Ting, M., and P. D. Sardeshmukh, 1993: Factors determining the extratropical response to equatorial diabatic heating anomalies. *J. Atmos. Sci.*, **50**, 907-918.

Wallace, J. M., and D. S. Gutzler, 1981: Teleconnections in the geopotential height field during the Northern Hemisphere winter. *Mon. Wea. Rev.*, **109**, 784-812.

Wang, B., 1988: Dynamics of tropical low-frequency waves: An analysis of the moist Kelvin wave. *J. Atmos. Sci.*, **45**, 2051-2065.

Wang, B., and H. Rui, 1990: Dynamics of the coupled moist Kelvin-Rossby wave on an equatorial β plane. *J. Atmos. Sci.*, **47**, 397-413.

Wright, P. B., J. M. Wallace, T. P. Mitchell and C. Deser, 1988: Correlation structure of the El Niño\Southern Oscillation phenomenon. *J. Climate*, **1**, 609-625.

Zhang, Z., 1988: The linear study of zonally asymmetric barotropic flows. Ph.D. thesis, University of Reading, Reading, UK. 178pp. [Available from The British Library, Document Supply Centre, Boston Spa, Wetherby, West Yorkshire, United Kingdom.

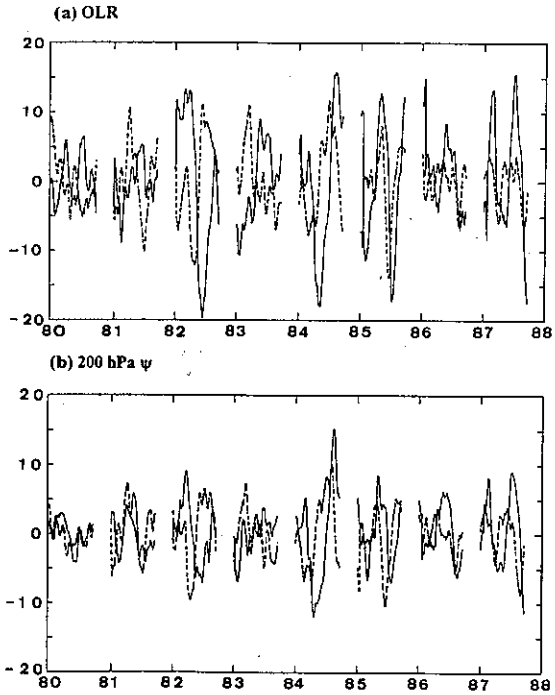

Fig 1. The expansion coefficients for the (a) OLR and (b) 200 hPa streamfunction vector of the first (solid line) and second (dashed line) mode for each winter from 1980/81 to 1987/88.

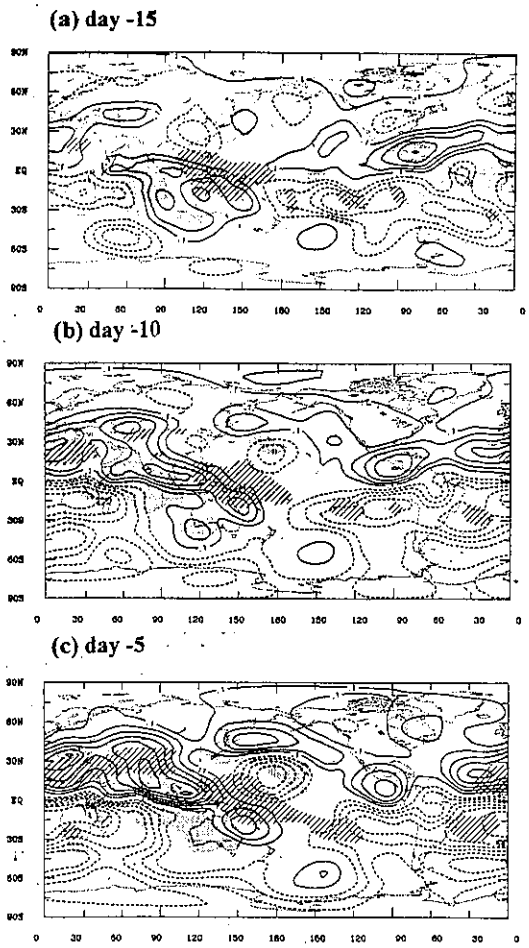

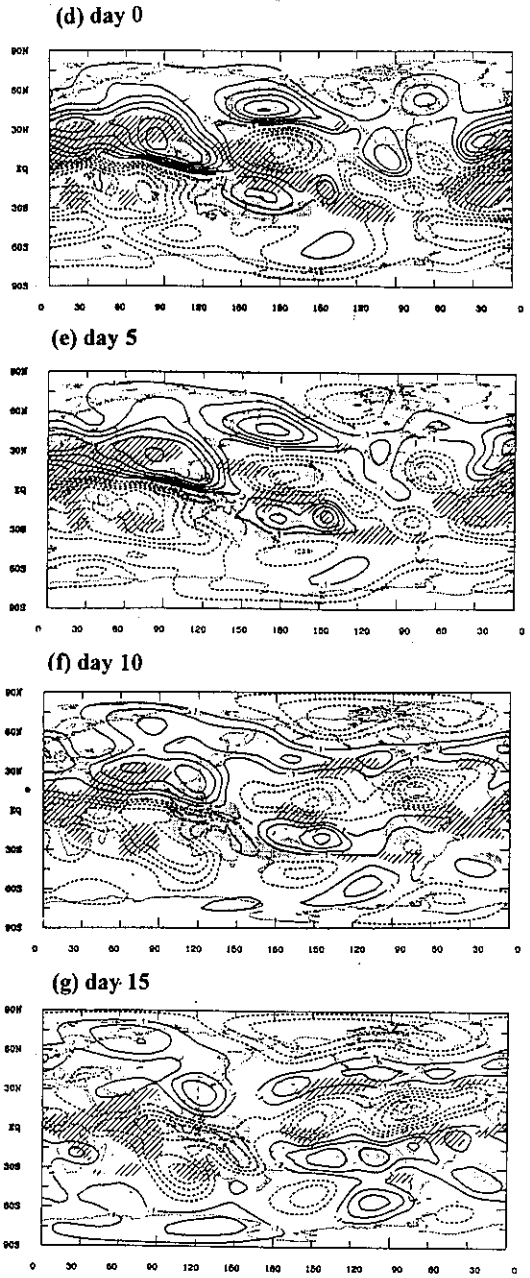

Fig 2. Correlation maps showing relationship between expansion coefficients of the first OLR vector and the 200 hPa streamfunction field at various time-lags: (a) day -15, (b) day -10, (c) day -5, (d) day 0, (e) day 5, (f) day 10, (g) day 15. The contour interval is 0.1; solid and dashed lines represent the positive and negative values, respectively. The zero value contour is not drawn. The corresponding OLR patterns are also shown in the shading scheme. Stippling indicates the areas where correlation coefficients are less than -0.2 while hatching indicates the areas where correlation coefficients are greater than 0.2.

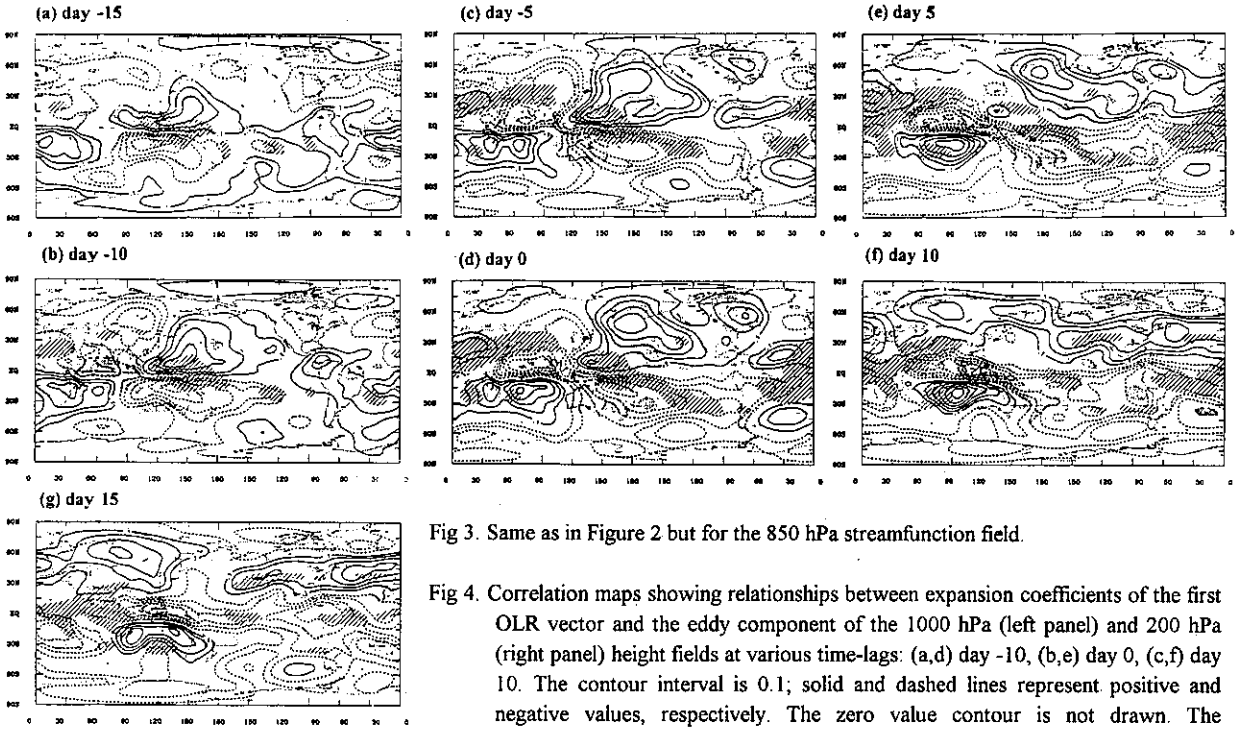

Fig 3. Same as in Figure 2 but for the 850 hPa streamfunction field.

Fig 4. Correlation maps showing relationships between expansion coefficients of the first OLR vector and the eddy component of the 1000 hPa (left panel) and 200 hPa (right panel) height fields at various time-lags: (a,d) day -10, (b,e) day 0, (c,f) day 10. The contour interval is 0.1; solid and dashed lines represent positive and negative values, respectively. The zero value contour is not drawn. The corresponding eddy OLR patterns are also shown in the same shading scheme as in Figure 2

Figure 4

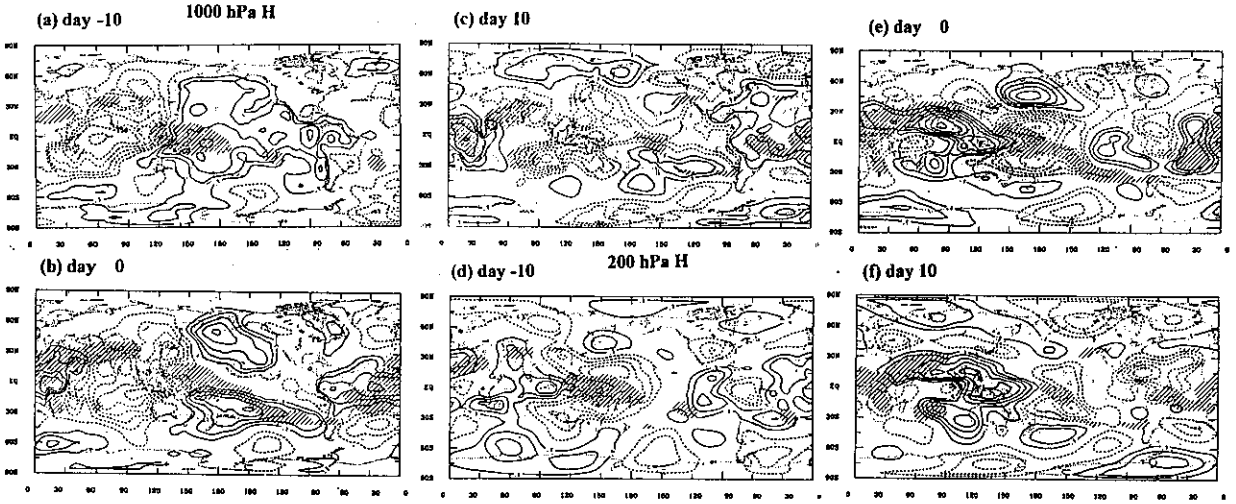

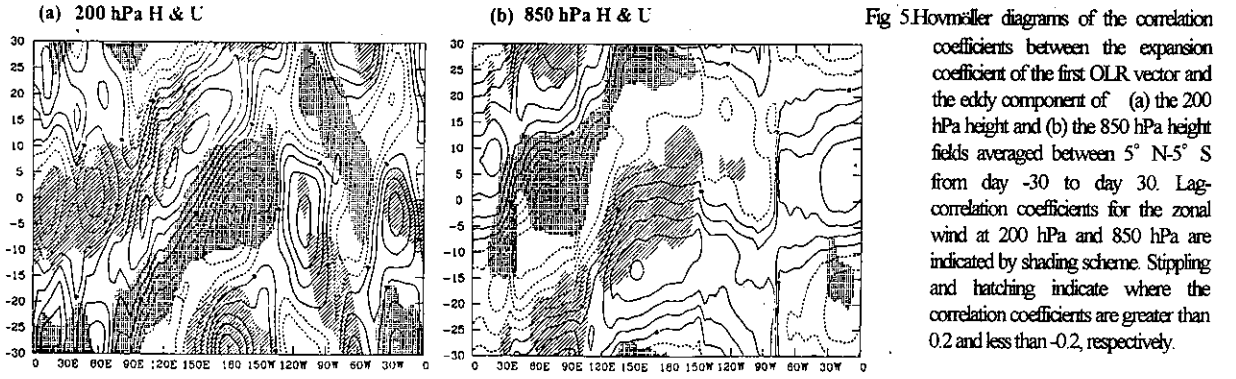

Fig 5.Hovmöller diagrams of the correlation coefficients between the expansion coefficient of the first OLR vector and the eddy component of (a) the 200 hPa height and (b) the 850 hPa height fields averaged between 5° N-5° S from day -30 to day 30. Lag-correlation coefficients for the zonal wind at 200 hPa and 850 hPa are indicated by shading scheme. Stippling and hatching indicate where the correlation coefficients are greater than 0.2 and less than -0.2, respectively.

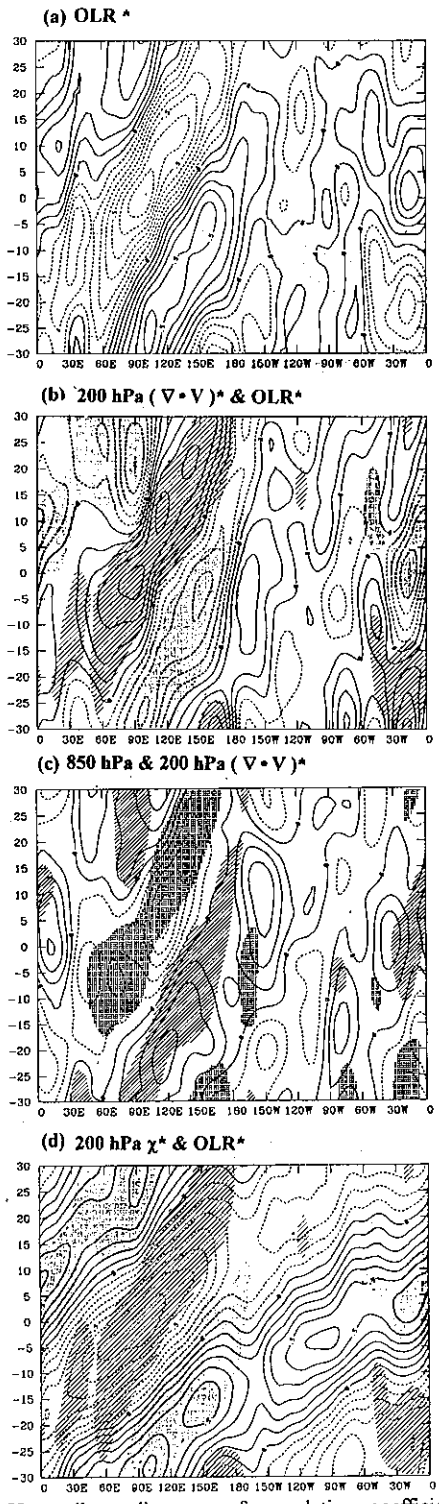

Fig 6. Hovmöller diagrams of correlation coefficients between the expansion coefficient of the first OLR vector and the eddy component of (a) OLR, (b) 200 hPa divergence (contoured) and OLR (shaded), (c) 850 hPa (contoured) and 200 hPa (shaded) divergence, and (d) 200 hPa velocity potential (contoured) and OLR (shaded), averaged from 5°N to 5°S and from day -30 to day 30. Stippling and hatching indicate where the correlation coefficients are greater than 0.2 and less than -0.2, respectively.

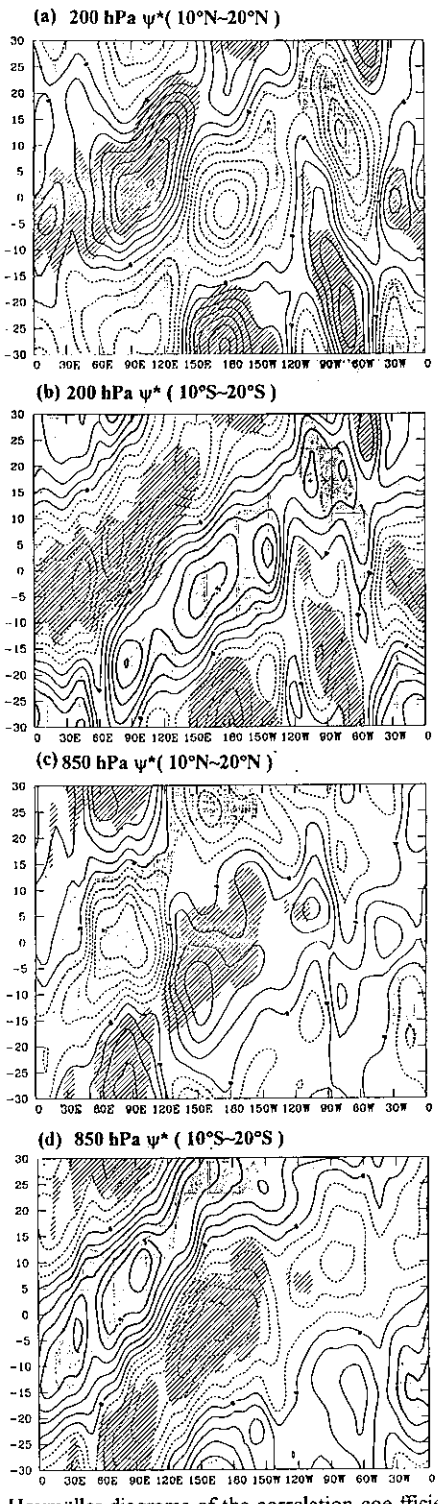

Fig 7 Hovmöller diagrams of the correlation coe-fficients between the expansion coefficient of the first OLR vector and the eddy component of (a) the 200 hPa streamfunction averaged between 10° N-20° N, and (b) the 200 hPa streamfunction averaged between 10° S-20° S, from day -30 to day 30. Stippling and hatching indicate where the correlation coefficients for the 200 hPa zonal wind, averaged between 5° N-5° S. are greater than 0.2 and less than -0.2. (C) and (d) are the same as (a) and (b) but for 850 hPa.

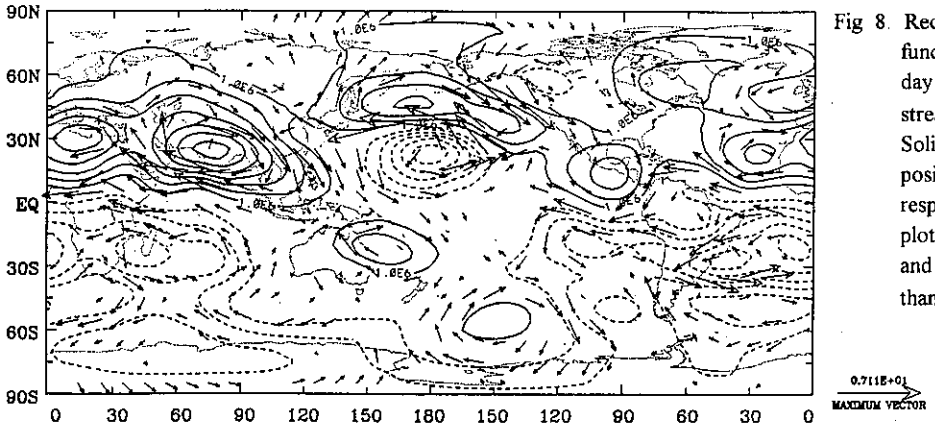

Fig 8. Reconstructed 200 hPa streamfunction and wind anomalies at day -5. Contour interval for streamfunction is 1×10^{6} m^2s^{-1}. Solid and dashed lines represent positive and negative values, respectively. Wind vectors are plotted only for every other point and where the amplitude is larger than 0.2 ms^{-1}.

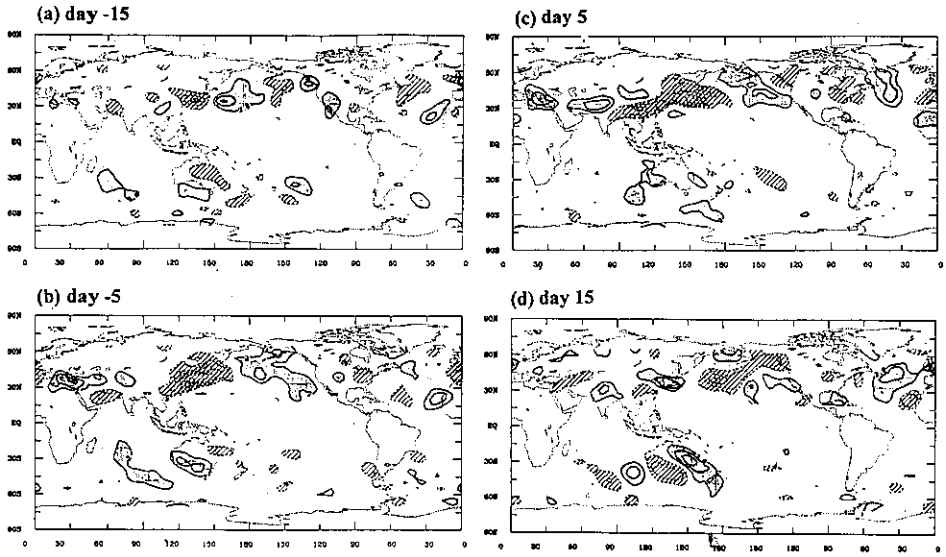

Fig 9. Rossby wave sources calculated from reconstructed wind anomalies at (a) day -15, (b) day -5, (c) day 5, and (d) day 15. The contour interval is 2 $\times10^{-11}$ sec^{-2}. Stippling and hatching indicate where the values are greater than 2×10^{-11} sec^{-2} and less than -2×10^{-11} sec^{-2}, respectively.

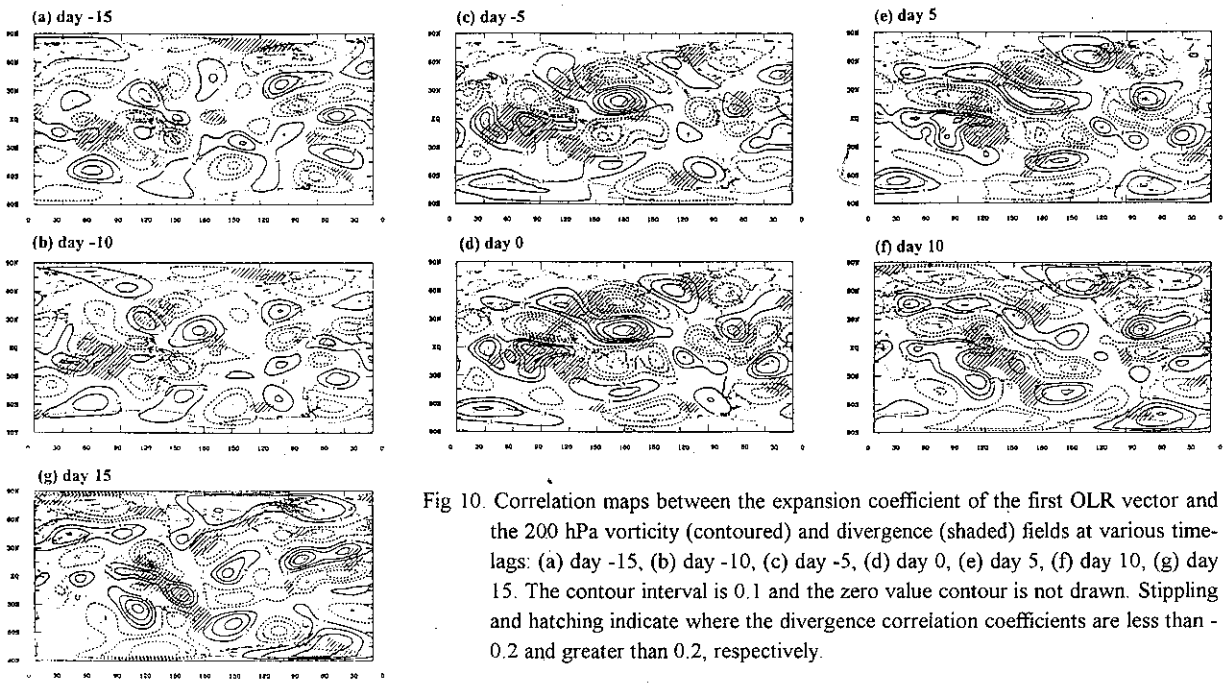

Fig 10. Correlation maps between the expansion coefficient of the first OLR vector and the 200 hPa vorticity (contoured) and divergence (shaded) fields at various timelags: (a) day -15, (b) day -10, (c) day -5, (d) day 0, (e) day 5, (f) day 10, (g) day 15. The contour interval is 0.1 and the zero value contour is not drawn. Stippling and hatching indicate where the divergence correlation coefficients are less than -0.2 and greater than 0.2, respectively.

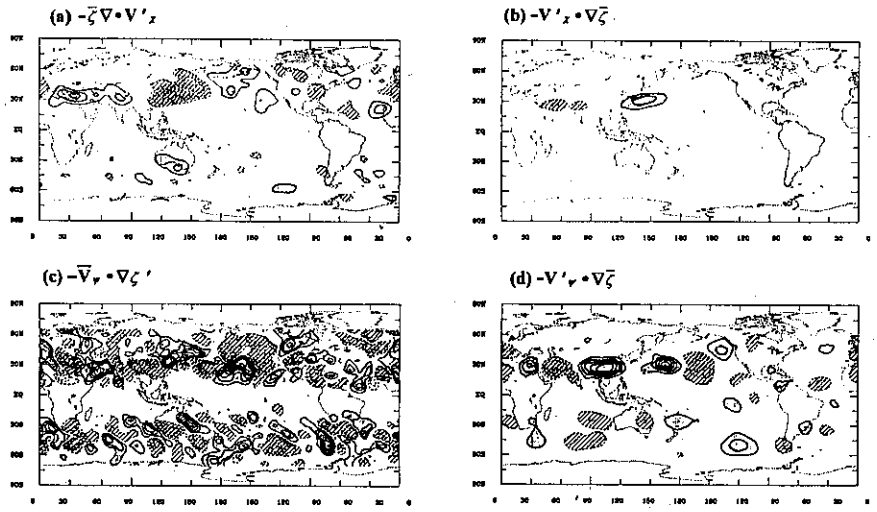

Fig 11. Plots of (a) $-\bar{\zeta}\nabla\cdot\mathbf{V}'_\chi$, (b) $-\mathbf{V}'_\chi\cdot\nabla\bar{\zeta}$, (c) $-\overline{\mathbf{V}_\psi}\cdot\nabla\zeta'$, (d) $-\mathbf{V}'_\psi\cdot\nabla\bar{\zeta}$ at 200 hPa for day -5. Contour interval is $2\times10^{-11}s^{-2}$ and the zero value contour is not plotted Areas of negative values are stippled.

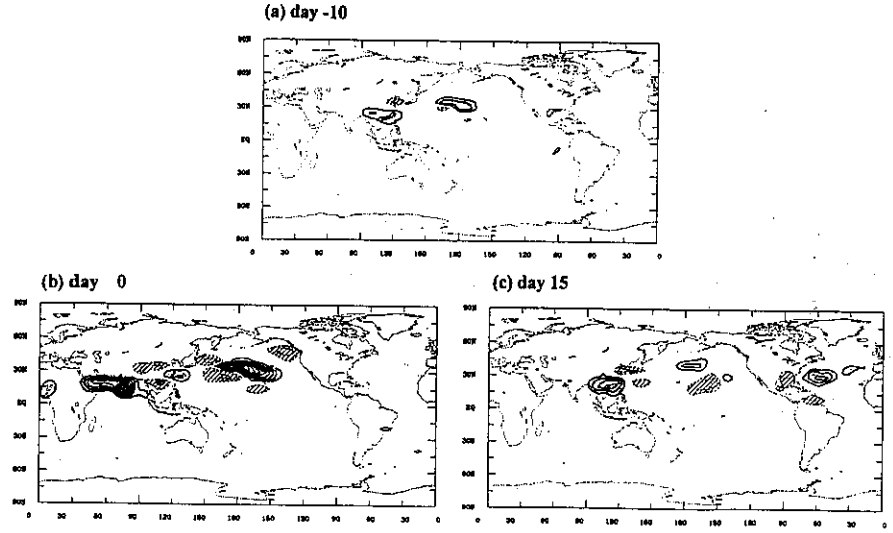

Fig 12. Kinetic energy conversion rates from mean flow to eddies calculated from the reconstructed wind anomalies at (a) day -10, (b) day 0, and (c) day 10. Contour interval is 5×10^{-5} J Kg^{-1} s^{-1} but the zero value contour is not drawn. Stippling and hatching indicate where the values are greater than 5×10^{-5} J Kg^{-1} s^{-1} and less than -5×10^{-5} J Kg^{-1} s^{-1}, respectively.

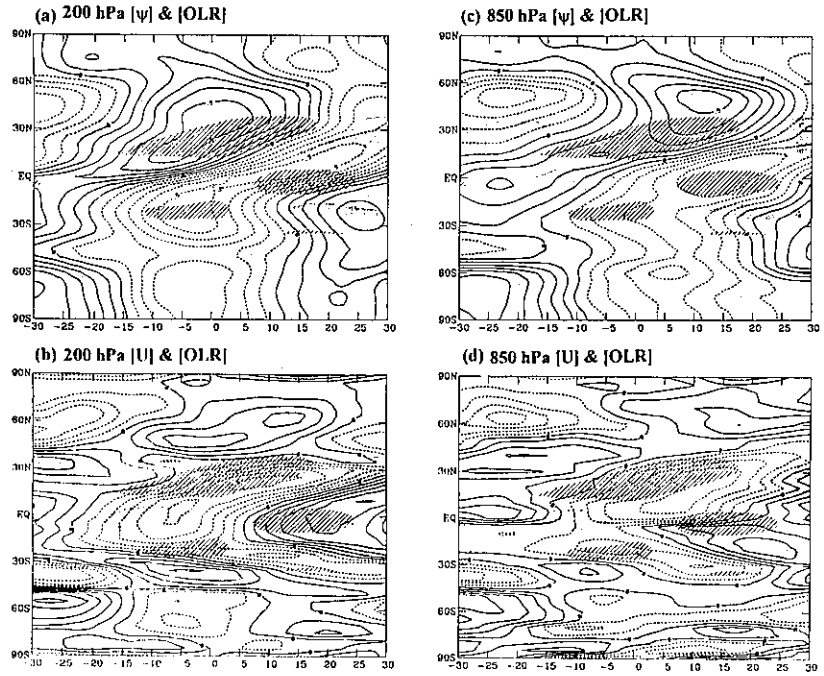

Fig 13. Hovmöller diagrams of the correlation coefficients between the expansion coefficients of the first OLR vector and the zonally averaged(a)200hPa stream-function, (b)200 hPa zonal wind, (c) 850hPa stream-function, and (d) 850hPa zonal wind fields from day -30 to day 30. The contour interval is 0.1. Stippling and hatching indicate where the correlation coefficients for the zonally averaged OLR are less than -0.2 and greater than 0.2, respectively.